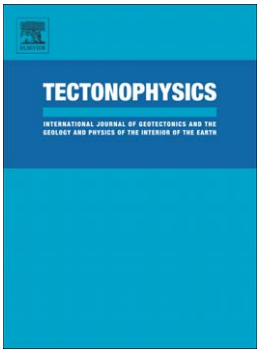

Applicability of magnetic fabrics in rocks associated with the emplacement of salt structures (the Bicorb-Quesa and Navarrés salt walls, Prebetics, SE Spain)

Ruth Soto, Elisabet Beamud, Belén Oliva-Urcia, Eduard Roca, Marc Rubinat, Juan J. Villalaín

PII: S0040-1951(14)00384-9
DOI: doi: 10.1016/j.tecto.2014.07.004
Reference: TECTO 126379

To appear in: *Tectonophysics*

Received date: 5 August 2013
Revised date: 19 May 2014
Accepted date: 2 July 2014

Please cite this article as: Soto, Ruth, Beamud, Elisabet, Oliva-Urcia, Belén, Roca, Eduard, Rubinat, Marc, Villalaín, Juan J., Applicability of magnetic fabrics in rocks associated with the emplacement of salt structures (the Bicorb-Quesa and Navarrés salt walls, Prebetics, SE Spain), *Tectonophysics* (2014), doi: 10.1016/j.tecto.2014.07.004

Applicability of magnetic fabrics in rocks associated with the emplacement of salt structures (the Bicorb-Quesa and Navarrés salt walls, Prebetics, SE Spain)

Ruth Soto[1*], Elisabet Beamud[2], Belén Oliva-Urcia[3], Eduard Roca[4], Marc Rubinat[4] and Juan J. Villalaín[5]

1 Instituto Geológico y Minero de España (IGME), Unidad de Zaragoza. C/ Manuel Lasala, 44, 9B, 50006 Zaragoza, Spain.
2 Laboratori de Paleomagnetisme CCiTUB-ICTJA CSIC. Institut de Ciències de la Terra "Jaume Almera", Solé i Sabarís, s/n, 08028 Barcelona, Spain.
3 Dpto. Geología y Geoquímica, Fac. Ciencias, Univ. Autónoma de Madrid. Campus Cantoblanco, 28049 Madrid, Spain
4 Institut GEOMODELS-Group of Geodynamics and Basin Analysis, Universitat de Barcelona, Zona Universitària de Pedralbes, 08028 Barcelona, Spain
5 Dpto. Física, Univ. Burgos, Av. Cantabria s/n, 09006 Burgos, Spain

*Corresponding autor. Tel.: +34 976 555 153; Fax: +34 976 553 358. *E-mail address:* r.soto@igme.es

Abstract

This work assesses the applicability of the analysis of the anisotropy of magnetic susceptibility (AMS) to rocks associated with salt structures. Magnetic fabrics from 16 sites sampled on Upper Triassic clays (Keuper facies) interbedded within the salt layers of the Bicorb-Quesa and Navarrés salt walls (Prebetic Zone, SE Spain) are mostly characterized by oblate magnetic ellipsoids with their magnetic foliation parallel to the bedding and magnetic lineation contained in the bedding plane but without a constant relationship with dip direction. To evaluate the quality and significance of the low-field AMS, several experiments were carried out to characterize the magnetic mineralogy of representative samples and enable separation of the contributions from paramagnetic and ferromagnetic (s.l.) minerals. The comparison between the orientation of the observed magnetic lineation and that of the structural elements characterizing the internal geometry of the studied salt structures (antiforms, minor folds, faults and shear zones) and flanks indicates that the magnetic fabric is controlled by deformation processes affecting the salt walls during their growth and/or evolution. Samples were

also analyzed from sixteen sites from Miocene rocks outcropping in several syn-diapiric Miocene half-grabens related to the salt walls studied. Their magnetic fabric is interpreted to reflect the dominant stretching direction at the syn-diapiric half grabens during and/or shortly after deposition. Our results indicate that caution is required in interpreting magnetic lineations related to salt flow mechanics from rocks associated with salt structures.

Keywords: magnetic fabrics, salt tectonics, salt wall, internal diapir structure, Betic Chain

1. Introduction

The analysis of the geometry of salt structures through direct and/or indirect methods has attracted substantial attention during the last three decades due to their importance as geological reservoirs. Less attention has been paid, however, to the study of the kinematics and/or internal fabric of this kind of structure mainly because of their high internal complexity. This complexity results from the presence of diapiric (salt) rocks, which undergo viscoelastic deformation under geological conditions (Weijermars et al., 1993). Studies dealing with the kinematic and mechanical evolution of salt structures have been based on the analysis of natural examples (e.g. Jackson and Talbot, 1986; Burliga, 1996), analogue models (e.g. Koyi, 1991, 1998; Vendeville and Jackson, 1992) or numerical models (e.g. Weinberg and Schmeling, 1992; Daudre and Cloetingh, 1994). The aim of this study was to assess the applicability of the analysis of the anisotropy of magnetic susceptibility (AMS), an excellent proven indicator of the mineral fabric of many types of rocks (e.g. Tarling and Hrouda, 1993), in rocks

associated with salt structures and interpret the resulting data exploring possible relationships between the internal fabric and the rising and emplacement of salt structures (i.e. salt flow patterns).

AMS studies yield different types of information depending on the geological context and type of rocks sampled: (1) in undeformed sedimentary rocks, magnetic fabric analyses can indicate the paleodirections of current flow in sediments (e.g. Ledbetter and Ellwood, 1980; Liu et al., 2001; Parés et al., 2007); (2) in weakly deformed sedimentary rocks, even those lacking visible markers of deformation, they record the initial stages of deformation both in compressional (Kissel et al., 1986; Mattei et al., 1997; Sagnotti et al., 1998, 1999; Parés et al., 1999; Larrasoaña et al., 2004) and extensional (Mattei et al., 1997, 1999; Sagnotti et al., 1994; Cifelli et al., 2004, 2005; Borradaile and Hamilton, 2004) settings; (3) in deformed rocks, the magnetic lineation indicates either the stretching direction in highly strained zones (e.g. Lamarche and Rochette, 1987; Hirt et al., 2000) or the intersection of bedding and cleavage planes (e.g. Borradaile and Tarling, 1981; Rochette and Vialon, 1984; Parés and Dinarès-Turell, 1993); (4) in plutonic rocks, magnetic fabric can provide either the direction of principal strains if they have undergone tectonic ductile deformation or information on magma emplacement processes (e.g. Cruden, 1990; Bouchez, 1997, 2000); and finally, (5) in lava flows and dykes, the magnetic fabric also provides information on emplacement processes (e.g. Cañón-Tapia, 2004 and references therein). The application of AMS analysis to rocks associated with salt structures has not been extensively investigated before, despite this type of structure being ubiquitous and able to form in all tectonic settings (i.e. under extensional, compressional and gravity-sliding processes) (e.g. Hudec and Jackson, 2007).

The Bicorp-Quesa and surrounding Middle-Upper Triassic salt structures, located in the most external part of the Prebetic Zone (Betic Chain, SE Spain), were selected as pilot structures to test the applicability of AMS analysis to rocks associated with salt tectonics given: (1) the presence of claystones/siltstones interbedded within the evaporitic layers inside the salt structure, which makes it possible to avoid the diamagnetic behavior of evaporitic rocks (the Km of Triassic evaporites being -11 $x10^{-6}$ SI; Rochette, 1987), and associated difficulties in interpreting AMS results; (2) their well-known internal geometry and deformational history deduced from very good outcrops and detailed field work (Roca et al., 1996; Rubinat et al., 2013), which allows comparison to results deduced from the magnetic fabric analysis; and (3) their magnetotelluric characterization, which makes it possible to infer their geometry at depth (Rubinat et al., 2010).

2. Geological setting

The structures chosen for this study, the Bicorb-Quesa and Navarrés salt-related structures, are located in the Prebetic Zone, the most external part of the fold and thrust belt of the Betic Chain (Fig. 1). The Prebetic Zone consists of a Mesozoic to middle Miocene cover detached above the Middle-Upper Triassic evaporites and clays from the Variscan basement (Vera, 1983). This cover is deformed by a series of folds, faults and diapirs mainly oriented ENE-WSW and also, locally, NNW-SSE (Fig. 1). These salt structures are composed of a thin basal evaporite layer (Röt facies); a 600-700 m thick succession of continental evaporites and fine clastics that are Upper Triassic in age (Keuper facies; Bartrina et al., 1990; De Torres and Sánchez, 1990). It can be divided into five stratigraphic units, from K1 to K5 (Ortí, 1974; De Torres and Sánchez, 1990;

Ortí and Pérez-López, 1994); a 50-200 m thick succession of Middle Triassic carbonates (Muschelkalk facies; Suarez Alba, 2007); and Triassic tholeitic dolerite sills (Martínez-González et al., 1997; Lago et al., 1999).

The Bicorb-Quesa salt-related structure (12 x 2 km) consists of a salt wall oriented ENE-WSW (Fig. 2). It is flanked by two syn-diapiric Miocene half-grabens, the Bicorb and Quesa half-grabens, to the north and south, respectively (Fig. 2). Towards the east, this structure continues with the NNW-SSE Navarrés salt wall (1 x 15 km), also bounded by two syn-diapiric Miocene half-grabens, the Escalona and Playamonte half-grabens, to the east and west, respectively (Fig. 2). Around these salt structures, most Jurassic and Cretaceous overburden rocks lie subhorizontally.

The Bicorb-Quesa and Navarrés salt walls result from a complex Alpine polyphase deformation history including three stages of successive extensional and contractional events (Roca et al., 1996, 2006; Rubinat et al., 2013); an initial Mesozoic extensional phase later deformed by an Early to Middle Miocene thin-skinned contractional deformation and, finally, a Late Miocene extensional phase. Magnetotelluric data have made it possible to infer the geometry of these salt structures at depth, and have evidenced that, at least, the Bicorb-Quesa salt wall is related to an N-dipping basement fault (the Bicorb-Quesa fault) oriented ENE-WSW and with a vertical displacement of 1000 m (Rubinat et al., 2010) (Fig. 2). Roca et al. (1996) previously pointed to the existence of this basement fault based on the observation of different thicknesses of the Cenomanian and Turonian materials around the Bicorb-Quesa salt wall; however, it was not possible to specify its location, displacement or orientation in any detail. The discovery of the N-dipping basement fault has highlighted the major role played by this fault in the initiation and reactivation of the Bicorb-Quesa salt wall in a thin-skinned Tertiary contractional setting (Rubinat et al., 2013). The presence of an

ENE-dipping basement fault beneath the Navarrés salt-wall segment has also been inferred from gravimetric (Carbó, 1982) and field data.

A detailed analysis of the internal structure of the Bicorb-Quesa and the northern Navarrés salt-wall segments shows that their development as salt walls was preceded by a contractional deformation that folded and faulted the Triassic rocks during the Paleogene-earliest Miocene building of the Iberian Range (Roca et al., 2013). The salt-wall growth occurred later during the late Miocene and linked to a thin-skinned extensional fault deformation. During this salt-wall development, the Triassic rocks were deformed by longitudinal large double-plunging antiforms, minor folds, vertical faults and shear zones (Roca et al., 2013).

3. Methodology; sampling and laboratory

Thirty-two sites were drilled in two different groups of rocks: 16 sites in red clays, Upper Triassic in age, outcropping inside the Bicorp-Quesa and the adjacent Navarrés salt walls (one site in K1, 8 sites in K2 and 7 sites in K3; see Table 1); and 16 sites in Miocene mudstones, clays and fine sandstones from the Bicorp and Quesa syn-diapiric half-grabens and other Miocene outcrops (see Fig. 2). In addition, nine sites were sampled in Jurassic and Cretaceous rocks located around the salt structures analyzed in this study, but AMS results were not interpretable. An average of eleven cores with different orientations was obtained in each site with a portable, water-cooled rock drill, and oriented in-situ with a magnetic compass. Low-field AMS at room temperature measurements were only made on one specimen per core. In order to minimize the possible effect of paleocurrents, all cores were sampled on clays and fine sandstones.

The low-field AMS was measured at room temperature (RT-AMS) using a static KLY-2 kappabridge susceptibility meter (AGICO) at the Paleomagnetic Laboratory of Barcelona CCiTUB-ICTJA CSIC. Magnetic susceptibility is a physical property of materials, representing the capacity of the material to be magnetized in a given magnetic field, and is described by a second-rank tensor (K) that relates the applied magnetic field (H) to an induced magnetization (M): M = K x H. The AMS at room temperature in rocks depends mostly on crystallographic preferred orientation, shape of grains, composition and sometimes the distribution-interaction of magnetic minerals (Tarling and Hrouda, 1993). Three axes define the susceptibility ellipsoid: maximum (k_{max}), intermediate (k_{int}) and minimum (k_{min}). The orientations of these axes correspond to the eigenvectors of the susceptibility tensors and characterize the magnetic fabric. The statistical procedure to obtain the directional and tensor data was based on Jelinek's method (Jelinek, 1977) using Anisoft 4.2 (Chadima and Jelinek, 2009). The magnetic fabrics have been described using parameters defined by Jelinek (1981): (1) the corrected anisotropy degree, P′, that provides a first indication of rock deformation and preferred mineral orientation, and (2) the shape parameter, T, ranging from -1 (prolate ellipsoid) to +1 (oblate ellipsoid).

In order to assess the quality and significance of the low-field AMS, we analyse the contributions from paramagnetic and ferromagnetic (s.l.) minerals to the total AMS. Two sites representative of Upper Triassic (QB18 with the highest Km value) and Miocene (QB08) rocks were analyzed by means of low-temperature AMS (LT-AMS) and anisotropy of the anhysteretic remanent magnetization (AARM) to compare their paramagnetic and ferromagnetic (s.l.) subfabrics, respectively. In addition, three more sites were analyzed by LT-AMS to better characterize the total AMS (the Upper Triassic QB03 site and the Miocene QB04 and QB19 sites). LT-AMS of spinning

specimens was measured in a KLY-3 kappabridge susceptibility meter (AGICO) in the Magnetic Fabric Laboratory at the University of Zaragoza. The samples were measured at 77 K (i.e. they were immersed in liquid nitrogen for one hour and for 10 minutes again between changing positions for the same sample) using the same method as in Parés and van der Pluijm (2002). Reducing the temperature of this type of sample generates an increase in the magnetic susceptibility, values at 77 K being approximately 3.8 times higher than at room temperature (298/77), assuming purely paramagnetic phases with a paramagnetic Curie temperature around 0 K (Lüneburg et al., 1999). This increase in the AMS at low temperature is not, however, symmetric along all axes, the k_{max} values increasing by a larger factor than k_{min} (Parés and van der Pluijm, 2002). A LT-AMS ellipsoid with the orientation and magnitude of its $k_{min} \leq k_{int} \leq k_{max}$ axes is also obtained from this kind of measurement and can be compared with results obtained at room temperature in order to estimate the paramagnetic contribution to the magnetic anisotropy (e.g. Richter and van der Pluijm, 1994; Parés and van der Pluijm, 2002).

The AARM was measured in four specimens per site. The anhysteretic remanent magnetization (ARM) was induced by a degausser with a DC field and the magnetization was measured in a SRM-755 cryogenic magnetometer (2G Enterprises) in the Paleomagnetic Laboratory at Burgos University. This procedure was performed along nine different axes for every sample. For each position, samples were previously demagnetized by alternating fields (AF) in a peak field of 100 mT and the remaining magnetization was measured. Subsequently, an ARM was induced in the sample by the application of a DC field of 0.05 mT together with a decreasing alternating field with a peak field of 90 mT. For each position, the remaining magnetization measured before the application of the ARM was subtracted. The AARM ellipsoid was calculated using

an algorithm programmed in a MS Excel provided by the Institute for Rock Magnetism, University of Minneapolis.

To characterize the ferromagnetic (s.l.) minerals that contribute to the magnetic susceptibility of the samples, several types of experiments were performed: (1) thermal demagnetization using the thermal demagnetizers TSD-1 (Schonstedt) and MMTD-80 (Magnetic Measurements) and a superconducting rock magnetometer SRM 755R (2G Enterprises) to measure the NRM, (2) isothermal remanent magnetization (IRM) acquisition up to 1.2 T, (3) three-axis IRM (in fields of 1.2, 0.3 and 0.1 T) thermal demagnetization as in Lowrie (1990) using an IM10-30 pulse magnetizer (ASC Scientific) and a TSD-1 thermal demagnetizer (Schonstedt), and (4) variation of magnetic susceptibility with temperature (K-T curves) of lutitic samples using a KLY3 susceptibility meter combined with a CS-L/CS-3 cryostat and furnace apparatus (all from AGICO). Two kinds of K-T curves were obtained: heating/cooling curves and low temperature measurements. The heating/cooling curves were acquired from room temperature to 700ºC and cooling back to room temperature in an argon atmosphere. The low temperature measurements were taken by cooling the samples to -190ºC and then heating them to room temperature in air. These K-T curves were also used to estimate the percentage of the paramagnetic/ferromagnetic (s.l.) content of the sample (Hrouda, 1994) using Cureval 8.0 software (Chadima and Hrouda, 2009). Additionally, the following three types of experiments were performed using a MMVFTB variable field translation balance (Magnetic Measurements)from powder of representative samples: (1) IRM acquisition curves, (2) backfield coercivity curves, and (3) hysteresis loops. Measurement of the NRM and the aforementioned IRM experiments were done in the Paleomagnetic Laboratory of Barcelona (CCiTUB-ICTJA CSIC), K-T curves in the Magnetic Fabric Laboratory at the University of Zaragoza and experiments done

with the variable field translation balance (MMVFTB) in the Paleomagnetic Laboratory at the University of Burgos.

4. Results

4.1. Magnetic properties and ferromagnetic (s.l.) mineralogy

On the basis of magnetic properties at room temperature, samples can be divided into two groups: (1) Group 1 is composed of the red clays Upper Triassic in age, and (2) Group 2 comprises the Miocene rocks that include brownish to grey clays and fine sandstones. The magnetic susceptibilities of the Group 1 samples range from 102 to 358 x 10^{-6} SI, being between 150 and 250 x 10^{-6} SI in the majority of specimens (Fig. 3), whereas Group 2 shows in general lower magnetic susceptibilities, most lying between 15 and 100 x 10^{-6} SI (except for site QB11 with values of 882-1409 x 10^{-6} SI) (see Fig. 3 and Table 1). In both groups, the magnetic ellipsoids were predominantly oblate (Fig. 4a and Table 1). Site-mean T values range between 0.3 and 0.9 in Group 1 samples, most of them indicating fabric ellipsoids that are clearly oblate (T>0.7) (Table 1), whereas in Group 2 samples range between -0.281 and 0.706 (except QB11), showing magnetic ellipsoids from clearly oblate to triaxial (T~0.0) to weakly prolate in shape. The corrected degree of anisotropy P' for both groups is low (Table 1), with values typical of weakly deformed sediments (P'<1.13). Group 1 samples (Triassic rocks) show a narrow range of Km with different degrees of anisotropy, suggesting different degrees of deformation, whereas Group 2 samples (Miocene rocks) show narrow ranges of both Km and P' values (Fig. 4b).

The analysis of the ferromagnetic (s.l.) mineralogy of the samples enabled us to distinguish the two aforementioned groups of rocks: (1) the Upper Triassic red beds, and (2) the Miocene brownish to grey clays and fine sandstones. The Upper Triassic red beds show maximum unblocking temperatures on the basis of the thermal demagnetization of the natural remanent magnetization (NRM) ranging between 550-690ºC. Their IRM curves are dominated by high coercivity minerals that are not saturated at 1 T and present remanence coercivity values of more than 300 mT (Fig. 5ad), suggesting that hematite is the main ferromagnetic (s.l.) carrier. The hysteresis loops of samples of this lithology are slightly wasp-waisted but show a typical hematite response (Fig. 5g). The temperature-dependent susceptibility curves (K-T curves) of these rocks also indicate that the final decay of the magnetic susceptibility occurs at 640ºC (Fig. 5j), consistent with the view that hematite is the main ferromagnetic (s.l.) phase (Petrovsky and Kapicka, 2006). These cooling curves are initially reversible (from approximately 660 to 590°C) but soon the susceptibility increases dramatically with respect to that observed in the heating run and magnetite is created probably from the reduction of hematite. In sample QB03.7a a sharp peak (Hopkinson) in the Tc of magnetite (Fig. 5j) was observed in the cooling run, suggesting a particular grain size of the ferromagnetic (s.l.) phase (e.g. Dunlop, 1974) and/or the creation of fine grain magnetite during heating.

Samples of Miocene clays and fine sandstones show a greater variety of magnetic carriers. In the pale samples (such as QB08 and QB59), the thermal demagnetization of the NRM shows maximum unblocking temperatures of around 550ºC in the low coercivity phase (0.1 T) and the IRM acquisition curves also point to magnetite being the main ferromagnetic (s.l.) carrier (Fig. 5ce). Miocene orange samples (such as QB04 and QB19) reached 550-670ºC before being thermally demagnetized and the IRM

curves show that a mixture of magnetite and hematite probably constitutes the main ferromagnetic (s.l.) minerals (Fig. 5bf). The hysteresis loops of Miocene samples also have a wasp-waisted shape, confirming this bimodal distribution of grains with contrasting coercivity (Fig. 5hi). The final decay of the magnetic susceptibility of these samples occurs at ~560-580ºC (Fig. 5kl). The cooling curves of these samples also show a dramatic increase in the susceptibility (Fig. 5kl).

In summary, the ferromagnetic (s.l.) mineralogy of the Triassic samples show a fairly homogeneous behavior, hematite being the main ferromagnetic (s.l.) carrier, and the Miocene samples present a greater variety, with magnetite together with different contributions from a high coercivity phase, probably hematite, as the main ferromagnetic (s.l.) carriers. Both Triassic and Miocene samples show variable proportions of paramagnetic with respect to ferromagnetic (s.l.) content, as reflected in the hyperbolic decay observed in the heating curves (Fig. 5jkl).

4.2. Low-temperature AMS and AARM

Samples analyzed by LT-AMS and AARM are all clays. They differ in color and age: red in the Upper Triassic samples and brownish (QB04 and QB19) and pale grey (QB08) in the Miocene samples. Regardless of these differences, the increase in bulk susceptibility at low temperature with respect to its value measured at room temperature is similar in all samples (Fig. 6a), the ratio between the bulk susceptibility at low and room temperature (LT/RT ratio) being around 2.2 in all samples (Fig. 6a). These LT/RT ratios indicate the predominance of the paramagnetic minerals controlling the AMS. Only samples from site QB03 (red bed) show a higher ratio (LT/RT=3.8) close to the perfect paramagnetic behavior. The shape of the LT ellipsoid is oblate in all cases

(T>0.5) (Fig. 6c and Table 2). These results are similar to that obtained at room temperature, with the exception of site QB08 that shows a triaxial magnetic ellipsoid (T=0.102, Table 1) with k_{min} and k_{int} axes girdling in a plane perpendicular to a fairly well clustered k_{max} at room temperature. As in the measurements at room temperature, both the bulk susceptibility and the corrected anisotropy degree (P') at low temperature were higher in the Upper Triassic red bed samples than the Miocene clays (Fig. 6c,b and Table 2).

The AARM ellipsoids display a different behavior depending on the site analyzed. Specifically, the axes of the AARM ellipsoid coincide with those of the RT-AMS for the Upper Triassic site (QB18), but they do not match for samples from the Miocene site (QB08) (Fig. 7). In fact, this disagreement could explain the better grouping of the k_{min} and k_{int} axes at low temperature than at room temperature for site QB08 (Fig. 7). In the case of the Triassic rocks, the three axes of the RT-AMS, LT-AMS and AARM ellipsoids coincide, suggesting that hematites (the main carrier of the ferromagnetic s.l. subfabric) have a similar subfabric to that shown by the paramagnetic minerals. For Miocene rocks, with a more variable ferromagnetic (s.l.) mineralogy, the axes of the RT-AMS and LT-AMS ellipsoids coincide in site QB19 (Fig. 7), but results from sites QB04 and QB08 point out the influence of a different ferromagnetic (s.l.) subfabric to the RT-AMS in those samples.

4.3. Magnetic fabric

Regardless of the rock type, color and age, all sites can be grouped into four types of magnetic ellipsoids according to their directional properties (Fig. 8 and Table 1). The first type (Fig. 8a), observed in 32% of the analyzed sites, is characterized by an oblate

magnetic ellipsoid with the minimum susceptibility axes (k_{min}) perpendicular to the bedding plane and the maximum (k_{max}) and intermediate (k_{int}) susceptibility axes scattered within the bedding plane. In this type of magnetic fabric, it is not statistically justifiable to identify a magnetic lineation based on the site-mean orientation of k_{max} axes as the semi-angle (ε_{12}) of the confidence ellipse around the k_{max} axes in the k_{max}-k_{int} plane is large (>42º). It is representative of a sedimentary fabric related to compaction. Type 1 ellipsoids have not been taken into consideration for further structural analysis. The second type (Fig. 8b) consists of clearly oblate to oblate-to-triaxial susceptibility ellipsoids which also have k_{min} axes perpendicular to the bedding. In this case, k_{max} and k_{int} are in the bedding plane and they are slightly more closely grouped than in the first type as indicated by smaller ε_{12} values (see Table 1). This indicates that, although weak, a magnetic lineation can be distinguished in these sites. Most sites sampled in the Upper Triassic rocks and three Miocene sites show this type of magnetic fabric (see Table 1). In the third type (Fig. 8c), again with a defined magnetic lineation in the bedding plane, the k_{min} and k_{int} axes are scattered forming a girdle perpendicular to k_{max}. Thus in this magnetic fabric type, the semi-angle (ε_{13}) of the confidence ellipse around the k_{min} axes in the k_{max}- k_{min} plane is larger (>42º) than in the two previous types. The magnetic ellipsoid is triaxial to weakly prolate in shape. Only Miocene sites display this type of magnetic fabric. The fourth group (9% of sampled sites) contains all the types of magnetic ellipsoids not covered by the last three types. It includes ellipsoids with k_{min} axes not perpendicular to the bedding plane, meaning that their magnetic foliation does not coincide with bedding, and also magnetic ellipsoids with a very high dispersion in the orientation of their magnetic axes. Like type 1, sites classified into this last group have not been taken into consideration for further structural interpretations. In addition, site QB11 has not been considered due to

its high magnetic susceptibility signal (Km=1140 x 10^{-6} SI), probably dominated by ferromagnetic (s.l.) minerals (as ferromagnetic s.l. minerals can have 2 to 3 orders of magnitude higher magnetic susceptibilities than paramagnetic minerals).

4.4. Orientation of the magnetic ellipsoids

Diapiric structure

For the magnetic ellipsoids of the Upper Triassic sites located in areas where the structure is relatively simple and consists of beds folded parallel to the salt-wall axis (sites QB07, QB10, QB15, QB56, QB60, QB62, QB66, and QB69), tectonic correction was performed by simple bedding plane restoration. In areas with superimposition of two differently-oriented trains of folds and local tilting, the tectonic correction was performed following the inverse sequence of tectonic events that were deduced, from field data, to have occurred at each site (see Table 1). In particular, six of these sites were affected by local tilting after the formation and rising of the salt structure and two sites were first folded and then tilted. Thus, the magnetic foliation of all sites is parallel to bedding (Fig. 9 and Table 1). All sites, except 4 at which the k_{max} and k_{int} axes are scattered within the bedding plane (i.e., magnetic fabric type 1; sites QB12, QB56, QB66 and QB69), have a type 2 magnetic fabric (see the previous section). As described above, the magnetic lineation of all type 2 sites is contained in the bedding plane; however, the relationships between the orientation of the magnetic lineation and the dip direction are highly variable (including down-, oblique- and perpendicular-dip magnetic lineations; Fig. 10) suggesting a composite origin for the magnetic fabric of rocks inside the salt structure. Neither the orientation of the magnetic lineation nor the

magnetic fabric parameters P' and T are controlled by either the sampled diapiric material (K2 to K5) or the bedding dip value. On the other hand, the orientation of the magnetic lineation of most sites is parallel to the flanks of the salt walls, which, in fact, reflects the orientation of the axes of the two sheared antiforms cored by Muschelkalk and Keuper K1 facies that characterize the central part of the the Bicorp-Quesa salt-wall segment (Fig. 9). These antiforms, interpreted as two salt diapirs with incipient bulbs, are fringed by outward-verging synclines and affected by near-vertical reverse faults and shear zones in areas with different amounts of salt inflation (Roca et al., 2013).

In order to investigate this potential relationship, we also analyze in detail the internal structure of the area of two of the three sites where magnetic lineation is not parallel to the flanks of the salt structure (sites QB01 and QB10) (see Fig. 11). Both areas display numerous structural elements indicating they underwent a complex deformation. Site QB01 is located close to a fault system oriented NE-SW and site QB10 close to a fold-and-thrust system oriented WNW-ESE (Fig. 11). In both cases, the magnetic lineation is oriented perpendicular to the closest thrust and/or fold indicating the local tectonic transport direction and that these structures probably control the orientation of the magnetic ellipsoids locally.

In summary, the magnetic foliation observed inside the studied salt walls is controlled by the bedding, being parallel to this plane in most cases. The orientation of the magnetic lineation is controlled by the existing structural elements; it is seen to be parallel to the axes of the antiforms arranged along the salt-wall axes or perpendicular to the trend of fold-and-thrust systems deforming areas locally (sites QB01 and QB10).

Syn-diapiric Miocene half-grabens

The magnetic fabric type of the Miocene sites is very variable with type 1, 2 and 3 magnetic ellipsoids (Table 1). After tectonic correction by simple bedding restoration, the magnetic lineation of most Miocene specimens is found to be subhorizontal and its orientation is spread across a wide range with a maximum oriented NW-SE (Fig. 9 and Table 1). Most sites with an identifiable magnetic lineation had a down-dip lineation (i.e. parallel to the dip direction) (Fig. 10) perpendicular or highly oblique with respect to the direction of the principal normal faults delimiting both the Bicorb and Quesa half-grabens (Fig. 9).

5. Discussion

5.1. Magnetic fabric origin inside the salt structures

All sites sampled on Upper Triassic rocks and, therefore, inside the salt structures of the study area, have type 1 (sedimentary fabric related to compaction) or 2 (oblate to triaxial) magnetic ellipsoids, with exception of sites QB02 and QB60 (both being type 4) (Fig. 8 and Table 1). Despite these magnetic ellipsoids being very similar to those described for other weakly deformed rocks (e.g. Borradaile and Tarling, 1981; Mattei et al., 1997; Parés et al., 1999; Cifelli et al., 2004; Larrasoaña et al., 2004), the orientation of the magnetic lineation with respect to bedding is highly variable (down-, oblique- and perpendicular-dip magnetic lineations; Fig. 10). Magnetic lineations are usually normal to the shortening direction in compressional settings (e.g. Hrouda, 1982; Mattei et al., 1997) and perpendicular to normal faults in extensional basins (e.g. Mattei et al., 1997; Cifelli et al., 2005). This tendency implies, in simple cases without out-of-plane deformation, easily distinguishable patterns of magnetic lineation with respect to

bedding: perpendicular-dip and down-dip magnetic lineations in compressional and extensional settings, respectively. Inside the Bicorb-Quesa salt structure, the simultaneous occurrence of down-, oblique- and perpendicular-dip magnetic lineations with respect to bedding (Fig. 10) suggests the superposition of different tectonic events (e.g. Soto et al., 2003) and/or the superposition of different subfabrics which are the result of distinct processes (e.g. Borradaile and Jackson, 2004; Oliva-Urcia et al., 2009; Hirt and Almqvist, 2012) as the origin of the observed total magnetic fabric. We can rule out this latter possibility as our findings show that the total AMS reflects the paramagnetic subfabric in all rocks sampled. Further, in the Upper Triassic red beds, their ferromagnetic (s.l.) subfabric dominated by hematites coincides with the paramagnetic one, confirming that the superposition of different subfabrics is not the cause of the observed magnetic fabric.

The parallelism between the orientation of the observed magnetic lineation from most Triassic sites and the trend of the axes of the large antiforms and flanks of the salt structures seems to indicate a common origin, probably due to deformation related to the salt-wall growth and/or development during the late Miocene. During the salt-wall growth and/or development, strong internal deformation occurred, characterized by the formation of large antiforms flanked by minor upright folds, vertical faulting and formation of shear zones in areas with different amounts of salt inflation (Roca et al., 2013). This complex deformation history could be responsible for the observed magnetic fabrics without a clear pattern in the relationships between the magnetic lineation and bedding and that with respect to tectonic elements. To find this kind of magnetic fabrics when all minerals present the same orientation (i.e. same magnetic subfabric orientation) may be a diagnostic feature indicating the occurrence of several deformative events.

5.2. Magnetic fabric origin in related syn-diapiric half-grabens

With respect to the Miocene rocks from the associated syn-diapiric half-grabens, these samples show examples of all four types of magnetic ellipsoids found in the study area (Fig. 8 and Table 1). Most Miocene sites have a magnetic lineation perpendicular or highly oblique to the bedding strike (i.e. parallel to the dip direction) (Fig. 10). This disposition is common in extensional basins, where the magnetic lineation is generally orthogonal to the orientation of the main basin-bounding normal faults and parallel to the stretching direction of the basin (as well as parallel to the σ_3 axis determined from mesostructural analysis) (e.g. Sagnotti et al. 1994; Borradaile and Hamilton 2004; Mattei et al., 1997; Cifelli et al., 2005). Therefore, we interpret the magnetic lineation of the Miocene sites as the dominant stretching direction at the half grabens during and/or shortly after deposition of the sampled rocks. The fact that the maximum of k_{max} is oriented NW-SE (Fig. 9) and perpendicular to the NE-SW orientation of the two principal normal faults delimiting the two syn-diapir half-grabens flanking the Bicorb-Quesa diapir also supports this origin.

5.3. Magnetic fabric in rocks associated with salt structures

Most studies related to salt structures have dealt with the characterization of their external geometry and mechanics of formation (e.g. Jackson and Talbot, 1986; Koyi, 1998) and the geometry and kinematics of related salt-structures generated in the sedimentary overburden (e.g. Alsop, 1996; Buchanan et al., 1996). However, much less attention has been paid to their internal fabric (e.g. Kupfer, 1968; Talbot and Jackson,

1987; Jackson and Talbot, 1989; Miralles et al., 1996). One method that can be used to characterize even very subtle rock fabrics is AMS analysis (e.g. Tarling and Hrouda, 1993). This has been applied to the study of salt structures in non-scaled analogue models of diapir-like structures, shedding light on salt flow and internal strain patterns during the ascent of non-linear viscous material (Kratinová et al., 2006).

Applied to natural examples, only Smíd et al. (2001) have preliminarily used the analysis of the AMS in a salt dome from the Zagros Mts., obtaining information related to salt flow mechanics. In that case, the magnetic foliation coincided with the mesoscopic salt flow foliation and the direction of the magnetic lineation showed a wide variety of relationships to the magnetic foliation orientation that the authors interpreted in terms of salt flow mechanics. There are two key differences between this natural example and the rocks analyzed in the present study that do not favor a direct comparison between the results. (1) In the salt dome studied by Smíd et al. (2001) they sampled salt with different quantities of dispersed magnetic particles coming from volcanic and sedimentary rocks, among which hematite (i.e. ferromagnetic s.l. mineral) is interpreted as the main carrier of susceptibility, whereas in our study, we sampled red clays interbedded within the evaporitic layers in which the paramagnetic, ferromagnetic (s.l.) and total AMS ellipsoids present the same orientation. (2) The type and evolution of the salt structures studied are different. While that analyzed by Smíd et al. (2001) consists of a simple salt dome, the Bicorb-Quesa and Navarrés structures analyzed here are salt walls with a complex deformation history with several different tectonic episodes.

The correct identification of the magnetic carriers of the magnetic susceptibility is crucial in the study of rocks associated with salt structures as in other contexts since different minerals might form at different times and under different conditions (e.g.

Borradaile and Henry, 1997; Aubourg et al., 1991, 2000; Robion et al., 1999; Aubourg and Robion, 2002; Hirt *et al.* 2004; Oliva-Urcia *et al.* 2009; Hirt and Almqvist, 2012). The difficulty in interpreting salt fabrics by traditional methods lies in the rapid recrystallization of salt rocks, which removes the original fabric and can make it difficult to correctly determine the strain ellipsoids (Talbot and Jackson, 1987; Miralles et al., 2001). Therefore, the application of AMS analysis to the internal geometry of salt structures by studying salt rocks (e.g. halite) could be very successful and constitutes a powerful tool if they contain disseminated magnetic particles with a known origin. AMS analysis can be extended to the interbedded layers of non-salt rocks, as we have done in the selected natural example, if the orientation and origin of minerals controlling the magnetic fabric are known.

Special caution must be exercised in rocks associated with salt structures in terms of interpreting the observed magnetic lineations as being linked to salt flow mechanics. Our study reflects the importance of internal deformation processes inside the salt structure (folding, faulting and/or formation of shear zones related to salt structure growth and/or development) controlling the orientation of the observed magnetic lineation. Further AMS studies in salt tectonics are needed to explore the internal magnetic fabric of salt structures and the potential of AMS ellipsoids as salt flow markers.

6. Conclusion

In this work, we set out to assess the applicability of the AMS analysis in rocks associated with salt tectonics, not extensively investigated previously. With this objective, AMS analysis has been used to study: (1) the interbedded layers of Upper

Triassic clays (Keuper facies) outcropping inside the Bicorb-Quesa and Navarrés salt walls (Prebetic Zone, SE Spain), the geometry, kinematics and internal structure of which are well-known from previous studies, and (2) Miocene mudstones, clays and fine sandstones belonging to several related syn-diapiric Miocene half-grabens.

Inside the salt structures, the Upper Triassic red beds show the total magnetic fabric, the ferromagnetic (s.l.) subfabric dominated by hematites and the paramagnetic subfabric having similar orientations. The observed magnetic foliation in these rocks is always parallel to bedding and the orientation of the magnetic lineation very variable and related to deformation processes that occurred during the growth and/or evolution of the salt walls. The orientation of the magnetic ellipsoids of the Miocene rocks is interpreted in terms of it reflecting the dominant stretching direction at the syn-diapiric half grabens during and/or shortly after deposition of the sampled rocks.

Our results emphasize the importance of deformation processes controlling the magnetic fabric of rocks inside salt structures and alert us to the need to be cautious about assuming that salt flow is the only mechanism controlling the orientation of magnetic lineations observed in rocks inside salt structures.

Acknowledgements

Funding for this work came from projects CGL2010-21968-C02-01, CGL2010-21968-C02-02 and CGL2012-38481 of the Dirección General de Enseñanza Superior (DGES), Spanish Ministry of Economy and Competitiveness. Thanks to the Paleomagnetic Laboratory of Barcelona CCiTUB-ICTJA CSIC, the Magnetic Fabric Laboratory at the University of Zaragoza and the Paleomagnetic Laboratory at the University of Burgos

where the AMS and rock-mag analyses were carried out. We are grateful to the Editor, F. Martín-Hernández and an anonymous reviewer for their comments.

References

Alsop, G.I., 1996. Physical modelling of fold and fracture geometries associated with salt diapirism. In: Alsop, G.I., Blundell, D.J., Davison, I. (Eds.), Salt Tectonics. Geol. Soc. London Sp. Publ., 100, pp. 227-241.

Aubourg, C., Robion, P., 2002. Composite ferromagnetic fabrics (magnetite, greigite) measured by AMS and partial AARM in weakly strained sandstones from western Makran, Iran. Geophysical Journal International 151(3), 729-737.

Aubourg, C., Rochette, P., Vialon, P., 1991. Subtle stretching lineation revealed by magnetic fabric of Callovian-Oxfordian black shales (French Alps). Tectonophysics 185, 211-223.

Aubourg, C., Hebert, R., Jolivet, L., Cartayrade, G., 2000. The magnetic fabric of metasediments in a detachment shear zone: the example of Tinos Island (Greece). Tectonophysics 321, 219–236.

Bartrina, T., Hernández, E., Serrano, A., 1990. Estudio de subsuelo del Trias salino en la Depresión Intermedia. In: Ortí, F., Salvany, J.M. (Eds.), Formaciones evaporíticas de la Cuenca del Ebro y cadenas periféricas y de la zona de Levante. Nuevas aportaciones y guía de superficie. ENRESA e Universitat de Barcelona, Barcelona, pp. 232-238.

Borradaile, G.J., Tarling, D.H., 1981. The influence of deformation mechanism in magnetic fabrics of weakly deformed rocks. Tectonophysics 77, 151-168.

Borradaile, G.J., Henry, B., 1997. Tectonic applications of magnetic susceptibility and

its anisotropy. Earth Science Reviews 42, 49–93.

Borradaile, G.J., Hamilton, T., 2004. Magnetic fabrics may proxy as neotectonic stress trajectories, Polis rift, Cyprus. Tectonics 23, 1-11.

Borradaile, G.J., Jackson, M., 2004. Anisotropy of magnetic susceptibility (AMS): magnetic petrofabrics of deformed rocks. In: Martín-Fernández, F., Lüneburg, C., Aubourg, C., Jackson, M. (Eds.), Magnetic Fabric: methods and applications. Geological Society, London, Special Publication, 238, pp. 299-360.

Bouchez, J.L., 1997. Granite is never isotropic: an introduction to AMS studies of granitic rocks. In: Bouchez, J.L., Hutton, D., Stephens, W.E. (Eds.), Granite: From Segregation of Melt to Emplacement Fabrics, Kluwer, Dordrecht, pp. 95-112.

Bouchez, J.L., 2000. Anisotropie de susceptibilité magnétique et fabrique des granites, Comptes-Rendus de l'Académie des Sciences de Paris 330, 1–14.

Buchanan, P.G., Bishop, D.J., Hood, D.N., 1996. Development of salt-related structures in the Central North Sea: results from section balancing. In: Alsop, G.I., Blundell, D.J., Davison, I. (Eds), Salt Tectonics, Geol. Soc. London Sp. Publ. 100, pp. 111-128.

Burliga, S., 1996. Kinematics within the Klodawa salt diapir, central Poland. In: Alsop, G.I., Blundell, D.J., Davison, I. (Eds), Salt Tectonics, Geol. Soc. London Sp. Publ. 100, pp. 11-21.

Cañón-Tapia, E., 2004. Anisotropy of magnetic susceptibility of lava flows and dykes: A historical account. In: Martín-Fernández, F., Lüneburg, C., Aubourg, C., Jackson, M. (Eds.) Magnetic Fabric: methods and applications. Geol. Soc. London Sp. Publ. 238, 205-225.

Carbó, A., 1982. Estructura cortical del Levante Español en base a datos gravimétricos.

Revista de la Real Academia de Ciencias Exactas, Físicas y Naturales de Madrid 76, 365-378.

Chadima, M., Hrouda, F. 2009. Cureval 8.0: Thermomagnetic Curve Browser for Windows. www.agico.com.

Chadima, M., Jelinek, V. 2009. Anisoft 4.2, Anisotropy data browser for Windows. www.agico.com.

Cifelli, F., Mattei, M., Hirt, A.M., Gunther, A., 2004. The origin of tectonic fabrics in ‘‘undeformed’’ clays: the early stages of deformation in extensional sedimentary basins. Geophysical Research Letters 31, L09604, doi:10.1029/ 2004GL019609.

Cifelli, F., Mattei, M., Chadima, M., Hirt, A.M., Hansen, A., 2005. The origin of tectonic lineation in extensional basins: Combined neutron texture and magnetic analyses on "undeformed" clays. Earth and Planetary Science Letters 235, 62-78.

Cruden, A.R., 1990. Flow and fabric development during the diapiric rise of magma. Journal of Geology 98, 681–698.

Daudre, B., Cloetingh, S., 1994. Numerical Modeling of Salt Diapirism-Influence of the Tectonic Regime. Tectonophysics 240, 59-79.

De Torres, T., Sanchez, A., 1990. Espesores de las Facies Keuper en la Rama Castellana de la Cordillera Ibérica y en el Dominio Prebético. In: Ortí, F., Salvany, J.M. (Eds.), Formaciones evaporíticas de la Cuenca del Ebro y cadenas periféricas, y de la Zona de Levante. Nuevas aportaciones y guía de superficie. ENRESA e Universitat de Barcelona, Barcelona, pp. 212-218.

Dunlop, D.J., 1974. Thermal enhancement of magnetic susceptibility. J. Geophys. 40, 439–451.

Hirt, A.M., Almqvist, B.S.G., 2012. Unraveling magnetic fabrics. International Journal of Earth Sciences 101, 613-624.

Hirt, A.M., Julivert, M., Soldevila, J., 2000. Magnetic fabric and deformation in the Navia-Alto Sil slate belt, Northwestern Spain. Tectonophysics 320, 1-16.

Hirt, A.M., Lowrie, W., Lüneburg, C., Lebit, H.D., Engelder, T., 2004. Magnetic and mineral fabric development in the Ordovician Martinsburg Formation in the Central Appalachian fold and thrust belt, Pennsylvania. Martín-Fernández, F., Lüneburg, C., Aubourg, C., Jackson, M. (Eds.) Magnetic Fabric: methods and applications. Geol. Soc. London Sp. Publ. 238, 109-126.

Hrouda, F., 1982. Magnetic anisotropy of rocks and its application in geology and geophysics. Geophys. Surveys 5, 37-82.

Hrouda, F., 1994. A technique for the measurement of thermal changes of magnetic susceptibility of weakly magnetic rocks by the CS-2 apparatus and KLY-2 Kappabridge. Geophys. J. Int. 118, 604–612.

Hudec, M.R., Jackson, M.P.A., 2007. Terra infirma: Understanding salt tectonics. Earth Science Reviews 82, 1-28.

Jackson, M.P.A., Talbot , C.J., 1986. External shapes, strain rates, and dynamics of salt structures. Geological Society of America Bulletin 97, 305-323.

Jackson, M.P.A., Talbot , C.J., 1989. Anatomy of mushroom-shaped diapirs. Journal of Structural Geology 11 (1-2), 211-230.

Jelinek, V., 1977. The statistical Theory of Measuring Anisotropy of Magnetic Susceptibility of Rocks and its Application. Geofyzika, Brno 88 pp.

Jelinek, V., 1981. Characterization of the magnetic fabrics of rocks. Tectonophysics 79, 63-67.

Kissel, C., Barrier, E., Laj, C., Lee, T.Q., 1986. Magnetic fabric in “undeformed”

marine clays from compressional zones. Tectonics 5, 769-781.

Koyi, H., 1991. Mushroom diapirs penetrating overburdens with high effective viscosities. Geology 19(12), 1229-1232.

Koyi, H.A., 1998. The shaping of salt diapirs. Journal of Structural Geology 4, 321-338.

Kratinová, Z., Závada, P., Hrouda, F., Schulmann, K., 2006. Non-scaled analogue modelling of AMS development during viscous flow: A simulation on diapir-like structures. Tectonophysics 418, 51-61.

Kupfer, D.H., 1968. Relationship of internal to external structure of salt domes. In: Braunstein, J., O'Brien, G.D. (Eds), Diapirism and Diapirs, AAPG Memoirs 8, pp. 79-89.

Lago, M., Arranz, E., Galé, C., Bastida, C., 1999. Las doleritas toleíticas triásicas del sector SE de la Cordillera Ibérica: petrología y geoquímica. Estudios Geol. 55 (5-6), 223-235.

Lamarche, G., Rochette, P., 1987. Microstructural analysis and origin of lineations in the magnetic fabric of some Alpine slates. Tectonophysics 139 (3–4), 285–293.

Larrasoaña, J.C., Pueyo, E.L., Parés, J.M., 2004. An integrated AMS, structural, palaeo- and rock-magnetic study of Eocene marine marls from the Jaca-Pamplona basin (Pyrenees, N Spain); new insights into the timing of magnetic fabric acquisition in weakly deformed mudrocks. Martín-Fernández, F., Lüneburg, C., Aubourg, C., Jackson, M. (Eds.) Magnetic Fabric: methods and applications. Geological Society, London, Special Publication, 238, 127-143.

Ledbetter, M.T., Ellwood, B.B., 1980. Spatial and temporal changes in bottom-water velocity and direction from analysis of particle size and alignment in deep-sea sediment. Marine Geology 38, 245-261.

Liu, B., Saito, Y., Toshitsugu, Y., Abdeldayem, A., Oda, H., Hori, K., Zhao, Q., 2001.

Paleocurrent analysis for the Late Pleistocene–Holocene incised-valley fill of the Yangtze delta, China by using anisotropy of magnetic susceptibility data. Marine Geology 176, 175–189.

Lowrie, W., 1990. Identification of ferromagnetic minerals in a rock by coercivity and unblocking temperature properties. Geophysical Research Letters 17, 159-162.

Lüneburg, C.M., Lampert, S.A., Lebit, H.D., Hirt, A.M., Casey, M., Lowrie, W., 1999. Magnetic anisotropy, rock fabrics and finite strain in deformed sediments of SW Sardinia (Italy). Tectonophysics 307, 51-74.

Martínez González, R.M., Lago San José, M., Valenzuela Ríos, J.I., Vaquer Navarro, R., Salas, R., Dumitrescu, R., 1997. El volcanismo Triásico y Jurásico del sector SE de la Cadena Ibérica y sus relaciones con los estadios de rift mesozoicos. Bol. Geol. Min. 108, 367–376.

Mattei, M., Sagnotti, L., Faccenna, C., Funicello, R., 1997. Magnetic fabric of weakly deformed clay-rich sediments in the Italian peninsula: Relationship with compressional and extensional tectonics. Tectonophysics 271, 107-122.

Mattei, M., Speranza, F., Argentieri, A., Rossetti, F., Sagnotti, L., Funiciello, R., 1999. Extensional tectonics in the Amantea basin (Calabria, Italy): a comparison between structural and magnetic anisotropy data. Tectonophysics 307, 33-49.

Miralles, L., Sans, M., Pueyo, J.J., Santanach, P., 1996. Recrystallization salt fabric in a shear zone (Cardona diapir, southern Pyrenees, Spain). In: Vendeville, B., Mart, Y., Vigneresse, J.L. (Eds.), Salt, Shale and Igneous Diapirs in and around Europe, Geological Society, London, Special Publications 174, pp. 149-167.

Miralles, L., Sans, M., Galí, S., Santanach, P., 2001. 3-D rock salt fabrics in a shear zone (Súria Anticline, South-Pyrenees). Journal of Structural Geology 23 (4), 675-691.

Oliva-Urcia, B., Larrasoaña, J.C., Pueyo, E.L., Mata, P., Parés, J.M., Schleicher, A.M., Pueyo, O., 2009. Disentangling magnetic subfabrics and their link to deformation processes in cleaved sedimentary rocks from the Internal Sierras (west central Pyrenees, Spain). Journal of Structural Geology 31, 163-176.

Ortí, F., 1974. El Keuper del Levante español. Estudios Geológicos 30, 7-46

Ortí, F., Pérez-López, A., 1994. El Triásico Superior de Levante. III Coloquio de Estratigrafía y Paleogeografía del Pérmico y Triásico de España, Cuenca. Guía de campo. Alfredo Arche, Madrid.

Parés, J.M., Dinarès-Turell, J., 1993. Magnetic fabric in two sedimentary rock types from the Southern Pyrenees. Journal of Geomagnetism and Geoelectricity 45, 193-205.

Parés, J.M., van der Pluijm, B.A., 2002. Evaluating magnetic lineations (AMS) in deformed rocks. Tectonophysics 350, 283– 298.

Parés, J.M., van der Pluijm, B., Dinares-Turell, J., 1999. Evolution of magnetic fabrics during incipient deformation of mudrocks (Pyrenees, northern Spain). Tectonophysics 307, 1-14.

Parés, J.M., Hassold, N.J.C., Rea, D.K., van der Pluijm, B.A., 2007. Paleocurrent directions from paleomagnetic reorientation of magnetic fabrics in deep-sea sediments at the Antarctic Peninsula Pacific margin (ODP Sites 1095, 1101). Marine Geology 242, 261-269.

Petrovský, E., Kapička, A., 2006. On determination of the Curie point from thermomagnetic curves. J. Geophys. Res., 111, B12S27, doi:10.1029/2006JB004507.

Richter, C., van der Pluijm, B.A., 1994. Separation of paramagnetic and ferrimagnetic susceptibilities using low-temperature magnetic susceptibilities and comparison

with high field methods. Phys. Earth Planet. Inter. 82, 113-123.

Robion, P., Averbuch, O., Sintubin, M., 1999. Fabric development and metamorphic evolution of lower Palaeozoic slaty rocks from the Rocroi massif (French–Belgian Ardennes): new constraints from magnetic fabrics, phyllosilicate preferred orientation and illite crystallinity data. Tectonophysics 309 (1–4), 257-273.

Roca, E., Anadón, P., Utrilla, R., Vázquez, A., 1996. Rise, closure and reactivation of the Bicorb-Quesa evaporite diapir, eastern Prebetics, Spain. Journal of the Geological Society, London 153, 311-321.

Roca, E., Sans, M., Koyi, H., 2006. Polyphase deformation of diapiric areas in models and in the eastern Prebetics (Spain). AAPG Bulletin 90, 115-136.

Roca, E., Beamud, E., Rubinat, M., Soto, R., Ferrer, O., 2013. Paleomagnetic and inner diapiric structural constraints on the kinematic evolution of a salt-wall: The Bicorb-Quesa and northern Navarrés salt-wall segments case (Prebetic Zone, SE Iberia). Journal of Structural Geology 52, 80-95.

Rochette, P., 1987. Magnetic susceptibility of the rock matrix related to magnetic fabric studies. Journal of Structural Geology 9, 1015-1020.

Rochette, P., Vialon, P., 1984. Development of planar and linear fabrics in Dauphinois shales and slates (French Alps) studied by magnetic anisotropy and its mineralogical con-trol. Journal of Structural Geology 6, 33-38.

Rubinat, M., Ledo, J., Roca, E., Rosell, O., Queralt, P., 2010. Magnetotelluric characterization of a salt diapir: a case study on Bicorb-Quesa Diapir (Prebetic Zone, SE Spain). Journal of the Geological Society, London 167, 145-153.

Rubinat, M., Roca, E., Escalas, M., Queralt, P., Ferrer, O., Ledo, J.J., 2013. The influence of basement structure on the evolution of the Bicorb-Quesa Diapir

(eastern Betics, Iberian Peninsula): contractive thin-skinned deformation above a pre-existing extensional basement fault. International Journal of Earth Sciences 102, 25-41.

Sagnotti, L., Faccenna, C., Funiciello, R., Mattei, M., 1994. Magnetic fabric and structural setting of Plio-Pleistocene clay units in an extensional regime: the Tyrrhenian margin of central Italy. Journal of Structural Geology 16, 1243-1257.

Sagnotti, L., Speranza, F., Winkler, A., Mattei, M., Funiciello, R., 1998. Magnetic fabric of clay sediments from the external northern Apennines (Italy). Physics of the Earth and Planetary Interiors 105, 73-93.

Sagnotti, L., Winkler, A., Montone, P., Di Bella, L., Florindo, F., Mariucci, M.T., Marra, F., Alfonsi, L., Frepoli, A., 1999. Magnetic anisotropy of Plio-Pleistocene sediments from the Adriatic margin of the northern Apennines (Italy): implications for the time-space evolution of the stress field. Tectonophysics 311, 139-153.

Smíd, J., Schulmann, K., Hrouda, F., 2001. Preliminary data on the AMS fabric in salt domes from the SW part of Zagros Mts., Iran. Geolines 13, 114-115.

Soto, R., Mattei, M., Casas, A.M., 2003. Relationship between AMS and folding in an area of superimposed folding (Cotiella-Bóixols nappe, Southern Pyrenees). Geodinamica Acta 16, 171-185.

Suarez Alba, J., 2007. La Mancha Triassic and lower Lias stratigraphy, a well log interpretation. Journal of Iberian Geology 33, 55-78.

Talbot , C.J., Jackson, M.P.A., 1987. Internal kinematics of salt diapirs. AAPG Bulletin 71, 1068-1093.

Tarling, D.H., Hrouda, F., 1993. The Magnetic Anisotropy of Rocks. Chapman and Hall, London, 217 pp.

Vendeville, B.C., Jackson, M.P.A., 1992. The rise of diapirs during thin-skinned extension. Marine and Petroleum Geology 9, 331-353.

Vera, J.A., 1983. Las zonas externas de las cordilleras Béticas. In: Comba, J.A. (Ed.), Geología de España 2, Libro Jubilar J. M. Rios. IGME, Madrid, pp. 218-251.

Weijermars, R., Jackson, M.P.A., Vendeville, B., 1993. Rheological and tectonic modeling of salt provinces. Tectonophysics 217, 143-174.

Weinberg, R.F., Schmeling, H., 1992. Polydiapirs: multiwavelength gravity structures. Journal of Structural Geology 14 (4), 425–436.

Figure captions

-Figure 1. Regional geological map with the location of the study area. Black square indicates location of Figure 2.

-Figure 2. Geological map of the area studied and cross-section from field and geophysical (MT, magnetotelluric method) data (modified from Rubinat et al., 2010). Black squares represent location of maps in Figure 10.

-Figure 3. Histogram showing the values of Km of the Triassic and Miocene samples.

-Figure 4. (a) P'-T diagrams for the two different types of sampled rocks at room temperature. (b) Idem for mean susceptibility Km vs. degree of anisotropy P′.

-Figure 5. Representative examples of rock magnetic experiment results for Upper Triassic and Miocene samples. (a, b, c) Three-axis IRM demagnetization as in Lowrie (1990). (d, e, f) IRM acquisition (right) and backfield (left) coercivity curves. (g, h, i) Hysteresis loops. (j, k, l) Temperature-dependent susceptibility curves. Top: Heating-cooling curves measured in an argon atmosphere; bottom: low temperature runs in air .

-Figure 6. (a) Ratio between the magnetic susceptibility (Km) at low and room temperature (LT/RT) where LT/RT=3.8 corresponds to perfect paramagnetic behavior (Lüneburg et al., 1999). (b) Mean of the magnetic susceptibility (Km) at low temperature vs. the mean of the degree of anisotropy P' for five selected sites. (c) P'-T diagrams of the mean shape parameters of the ellipsoid of AMS measured at low temperature of the same selected sites.

-Figure 7. Stereoplots of the RT-AMS (left), LT-AMS (middle) and AARM (right) of representative sites. Lower-hemisphere equal-area stereoplots after tectonic correction.

-Figure 8. Examples showing the four typical magnetic ellipsoids found in the studied area and their P'-T diagrams. Orange great circles correspond to bedding planes. *In situ* lower-hemisphere equal-area stereoplots.

-Fig. 9. Simplified geological maps of the study area showing (a, b) the *in situ* magnetic foliation and lineation (only for type 2 and 3 magnetic fabrics) of Upper Triassic sites except for site QB11 (the magnetic fabric of which is probably dominated by ferromagnetic s.l. minerals, see text) and (c) the corrected magnetic lineation for type 2 and 3 magnetic fabrics in Miocene sites. Stereoplots inside (b) represent k_{max} (magnetic lineation) before and after tectonic correction for the Triassic rocks. Stereoplot inset in (c) represents k_{max} (magnetic lineation) before tectonic correction and density plots after tectonic correction for all Miocene sites (left) and only for Miocene sites with type 2 and 3 magnetic ellipsoids (right). Lower-hemisphere equal-area stereoplots in all cases.

-Fig. 10. (a) *In situ* lower-hemisphere equal-area stereoplots showing the relationships between the site mean directions of k_{max} and bedding. (b) Data for k_{max} and bedding have been rotated to align them with an N-S direction to facilitate comparisons.

-Fig. 11. Geological maps showing the detailed structure of the (a) northeastern flank and (b) southeastern flank of the Bicorb-Quesa salt wall, in relation to the orientation of the corrected magnetic lineation of sites QB01 and QB10 (adapted from Roca et al., 2013). See location on Figure 2. (c) *In situ* lower-hemisphere equal-area stereoplots of QB01 and QB10 with orientation of all magnetic axes and bedding.

-Table 1. Magnetic parameters measured at room temperature.

-Table 2. Magnetic parameters measured at low temperature (LT-AMS).

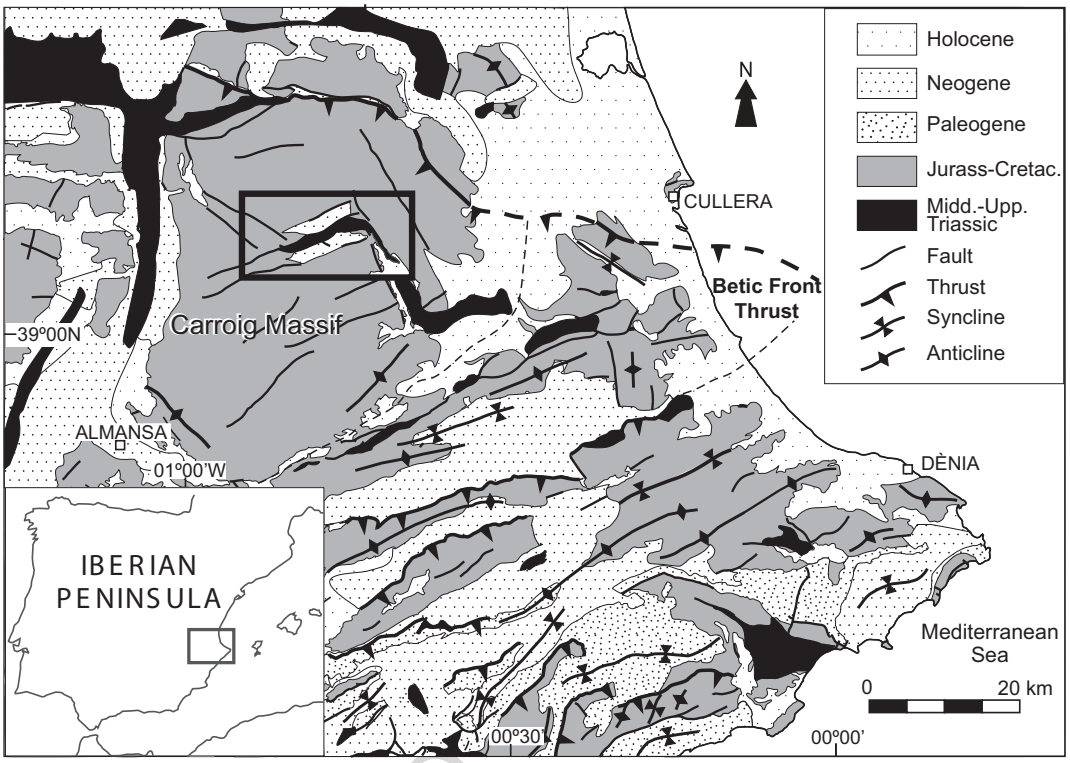

Figure 1

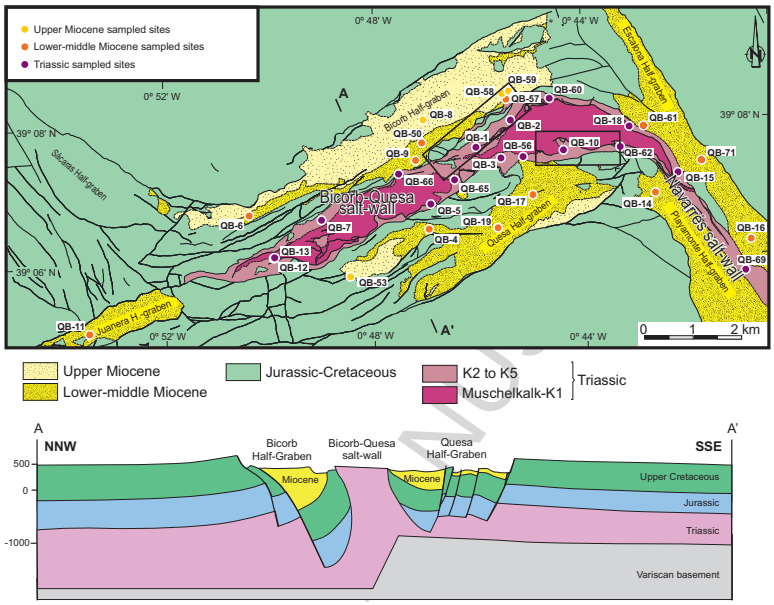

Figure 2

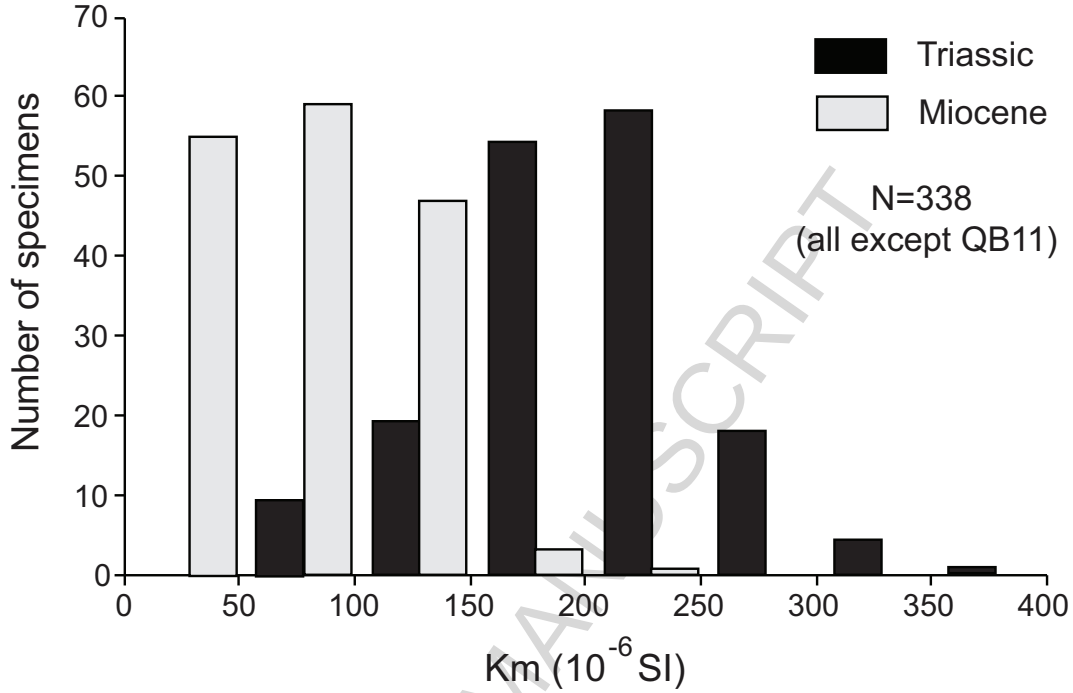

Figure 3

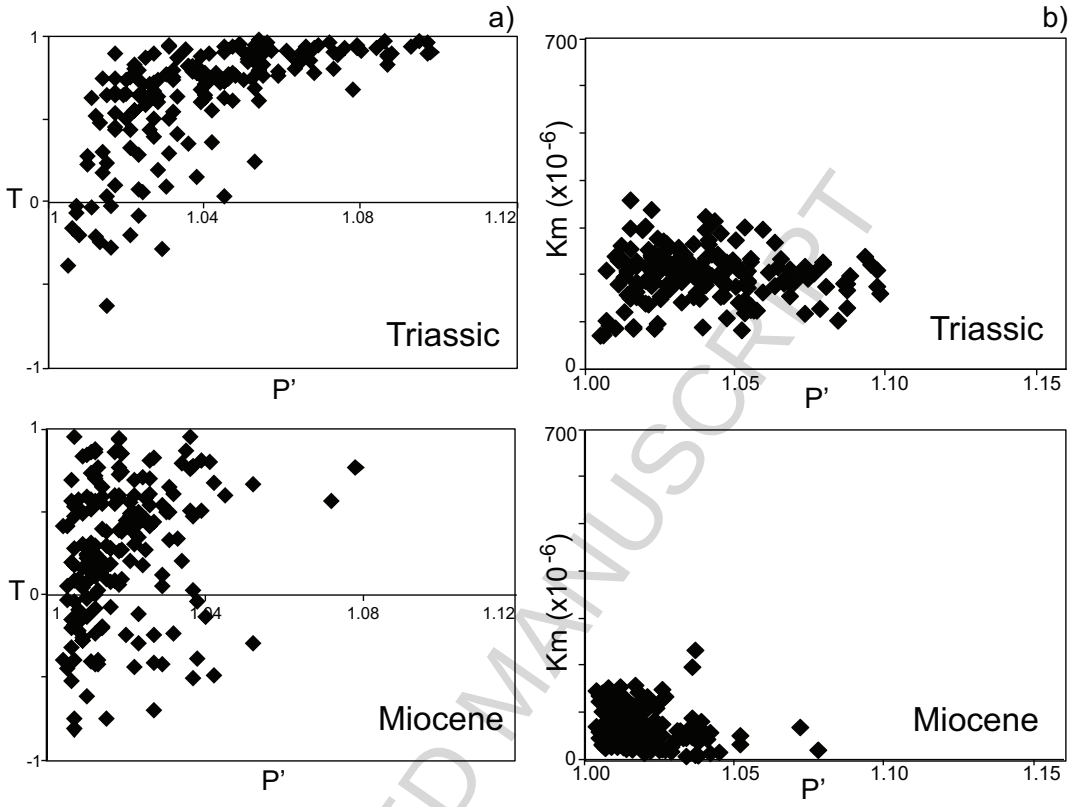

Figure 4

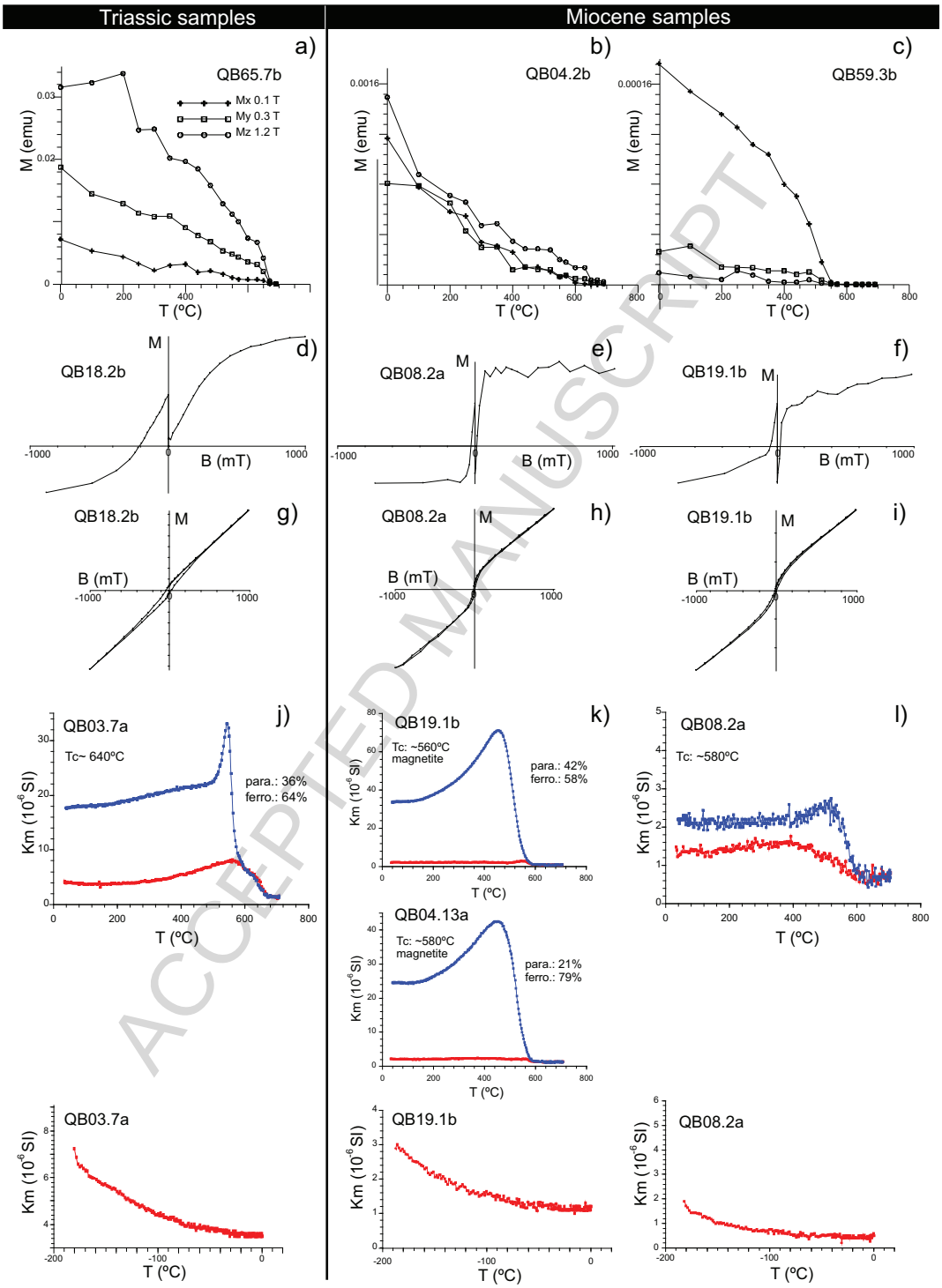

Figure 5

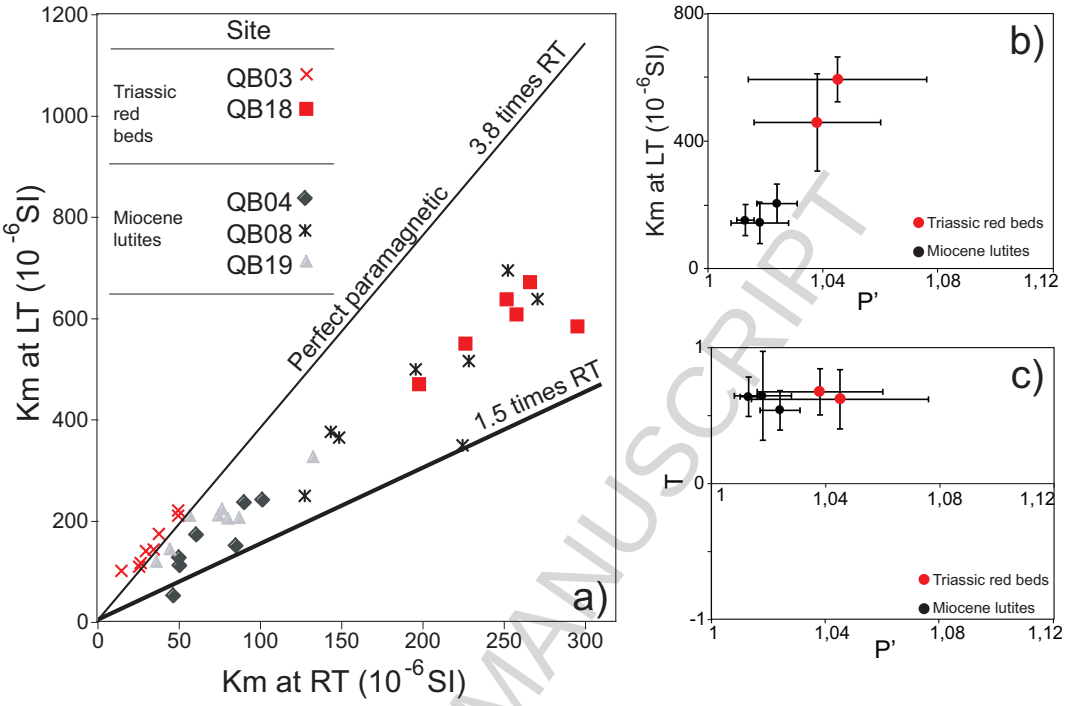

Figure 6

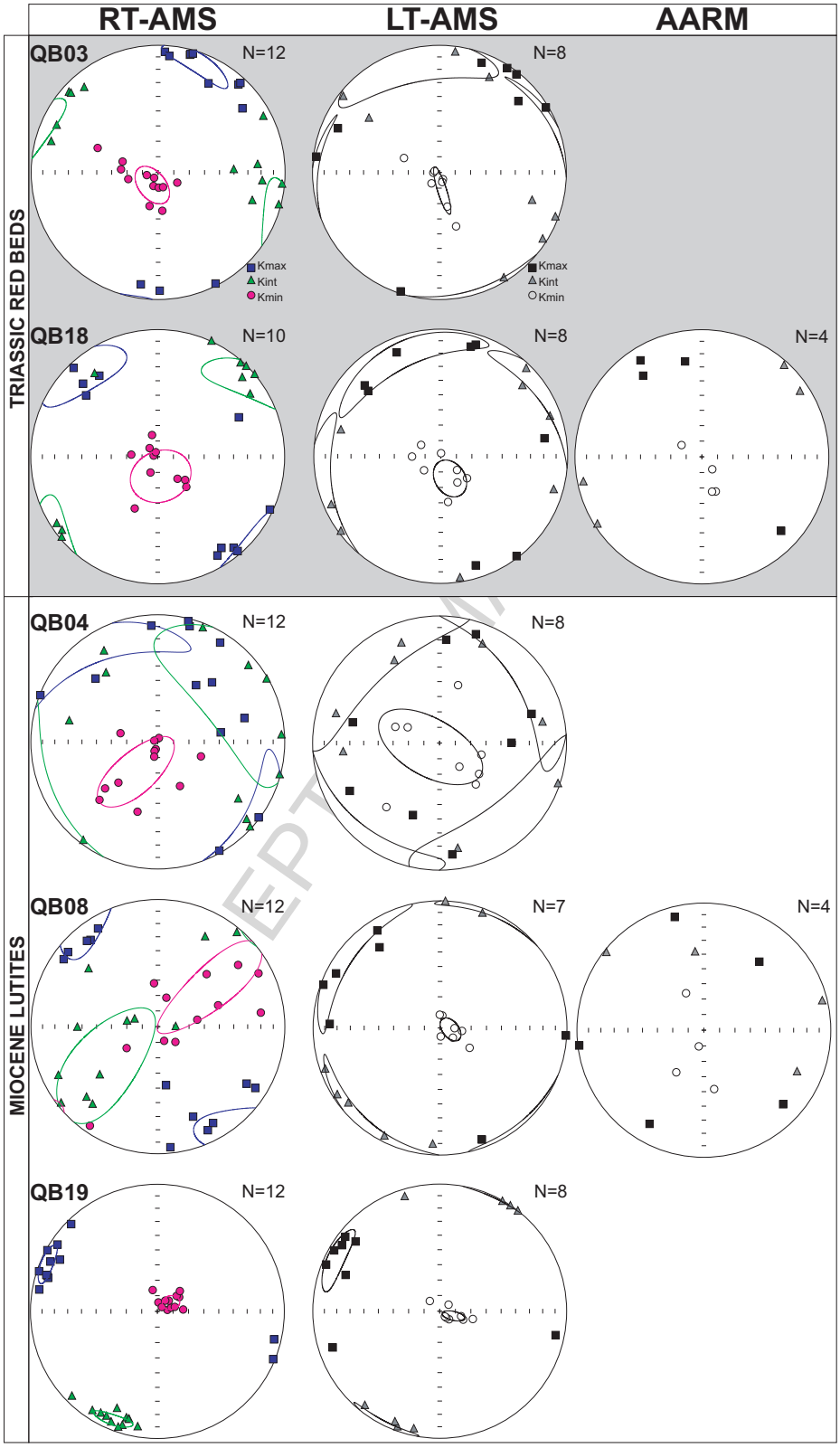

Figure 7

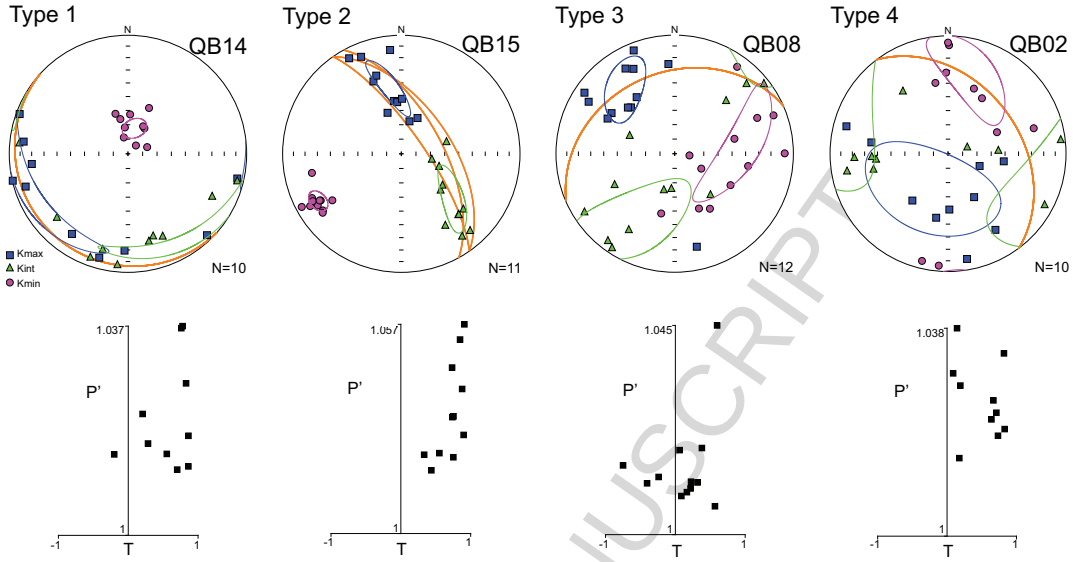

Figure 8

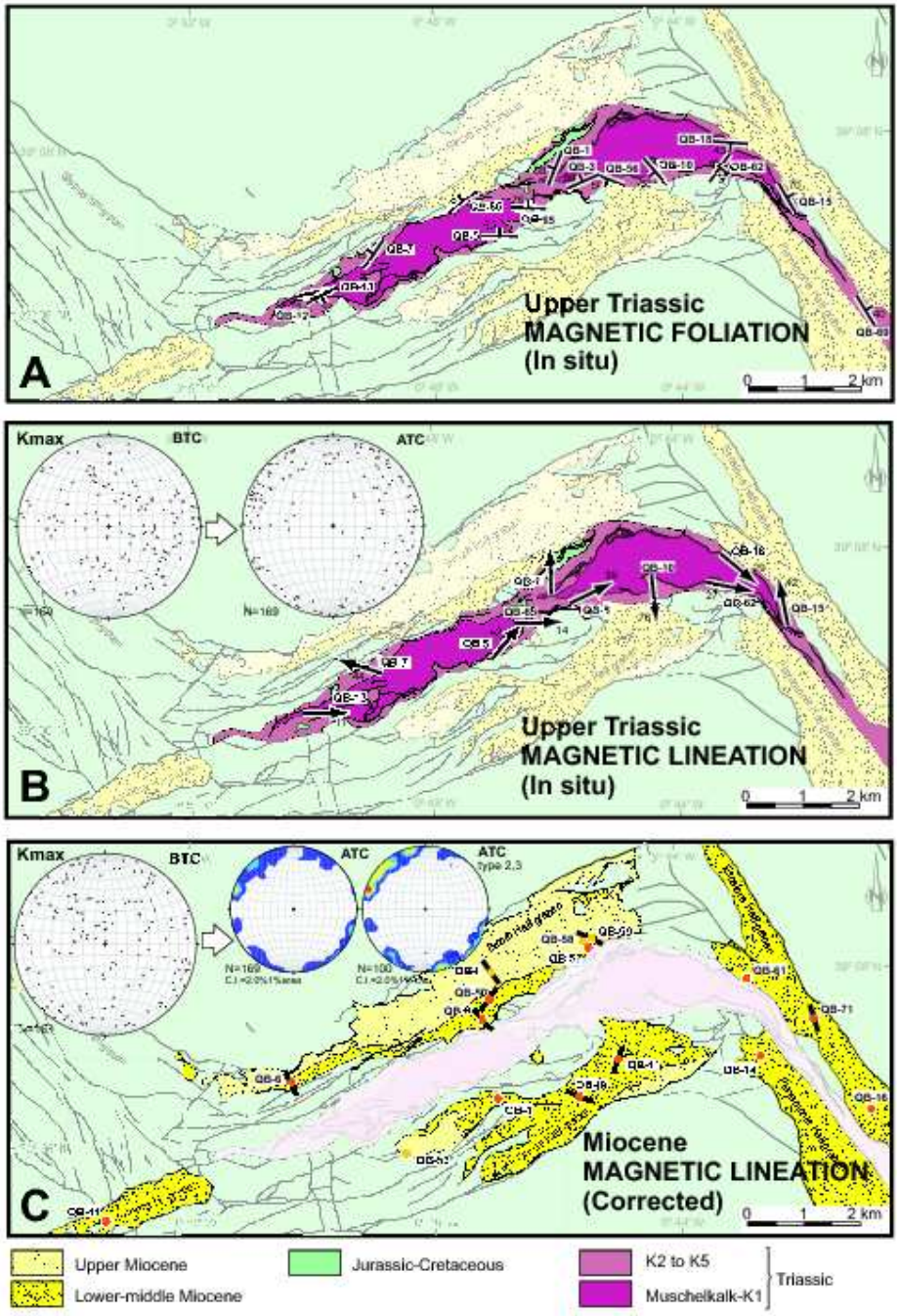

Figure 9

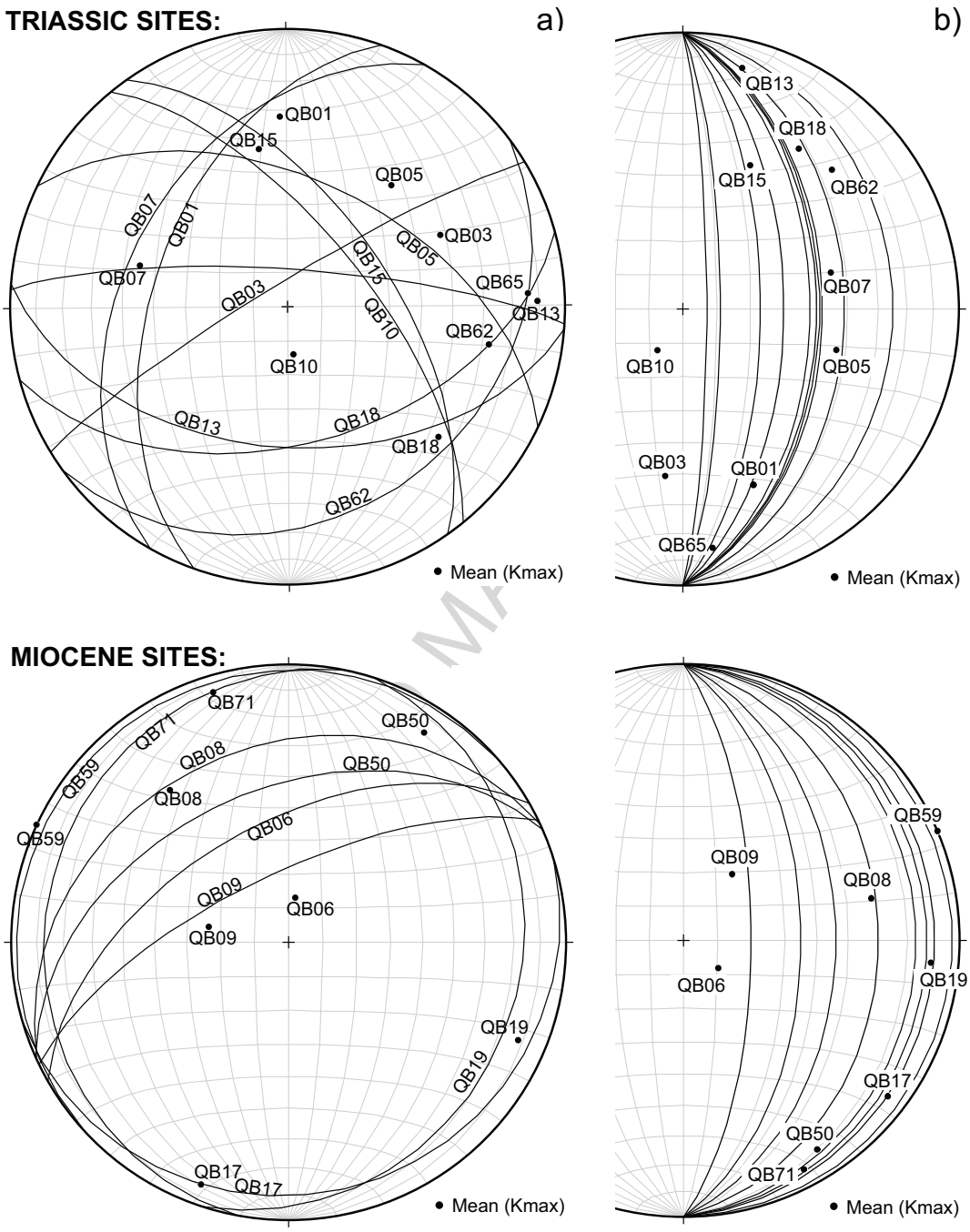

Figure 10

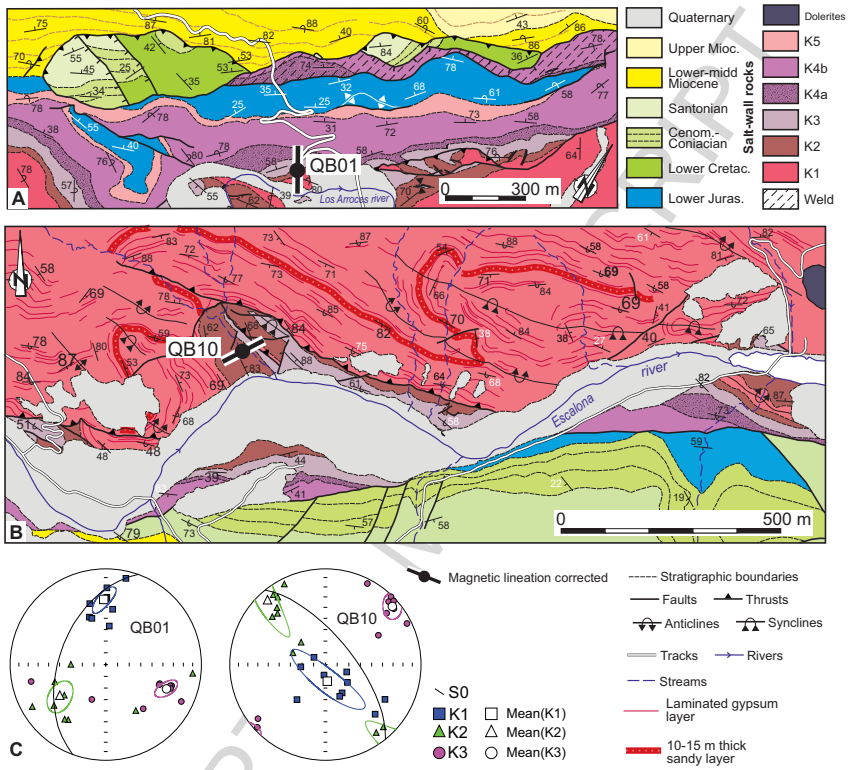

Figure 11

Table 1

Site	Lithology	Age	n	Km	P'	T	D,I(Kmax) In situ	E11.1 (e_{12}º/e_{13}º)	D,I(Kmax) Corrected	D,I(Kmim) In situ	E11.3 (e_{13}º/e_{23}º)	D,I(Kmin) Corrected	Magnetic ellip.Type	Bedding DD/Dip	Tectonic correction
Bicorb-Quesa and Navarrés salt-walls															
QB01	red lutites	Late Triassic-k2	9	224 (62.7)	1.032 (0.015)	0.356 (0.421)	358,32	14.6/5.3	330,6	112,32	10.8/5.5	112,82	2	290/50	b (fold axis 234/34)
QB02	red lutites	Late Triassic-k3	10	214 (20.2)	1.026 (0.007)	0.505 (0.306)	205,60	49/29.5	074,72	017,30	38.1/15.7	174,3	4	053/39	c (dip 310/70)
QB03	red lutites	Late Triassic-k2	12	185 (57.8)	1.046 (0.022)	0.658 (0.271)	065,39	19.8/7.6	310,9	156,2	13.8/8.7	126,81	2	329/83ov	b (fold axis 256/28)
QB05	red lutites	Late Triassic-k3	9	228 (57.1)	1.055 (0.025)	0.778 (0.169)	041,42	28.5/7.6	122,9	180,40	11.3/4.8	236,69	2	026/52ov	c (dip 340/60ov)
QB07	red lutites	Late Triassic-k2	10	214 (21.5)	1.063 (0.021)	0.883 (0.106)	286,44	28.4/3.4	117,0	124,45	4.5/2.2	027,75	2	300/41	a
QB10	red lutites	Late Triassic-k3	10	209 (33.5)	1.052 (0.023)	0.787 (0.119)	173,76	40.1/9.6	063,10	049,8	12.3/7.1	221,79	2	051/67	a
QB12	red lutites	Late Triassic-k2	12	196 (37.5)	1.042 (0.027)	0.655 (0.333)	204,26	58.0/12.6	027,9	334,53	17.5/7.0	165,78	1	155/49	c (dip 175/60)
QB13	red lutites	Late Triassic-k2	9	162 (53.5)	1.022 (0.015)	0.478 (0.385)	089,11	14.9/3.9	277,3	349,41	5.4/3.5	077,87	2	165/49	c (dip 175/60)
QB15	red lutites	Late Triassic-k3	11	174 (35.4)	1.033 (0.014)	0.713 (0.192)	350,42	25.5/5.6	013,3	240,20	7.1/6.0	263,82	2	055/60	a
QB18	red lutites	Late Triassic-k1	10	263 (42.5)	1.041 (0.027)	0.617 (0.263)	131,29	25.4/15.4	114,3	004,47	19.8/16.4	239,85	2	185/48ov	c (dip 225/60ov)
QB56	red lutites	Late Triassic-k2	17	135 (53.7)	1.023 (0.014)	0.228 (0.445)	231,54	51.4/21.6	255,8	022,32	47.7/23.1	096,81	1	fold	a
QB60	red lutites	Late Triassic-k3	10	260 (33.0)	1.031 (0.021)	0.625 (0.320)	057,84	34.1/6.6	031,20	301,3	8.7/5.6	122,1	4	028/64	a
QB62	red lutites	Late Triassic-k2	11	204 (31.0)	1.046 (0.009)	0.807 (0.122)	101,27	26.6/7.2	106,8	306,60	15.3/6.4	257,80	2	144/25	a

QB65	red lutites	Late Triassic-k2	11	186 (23.6)	1.063 (0.018)	0.865 (0.109)	087,14	40.8/8.2	027,4	181,14	11.2/4.4	245,86	2	004/79ov	c (dip 110/90)
QB66	red lutites	Late Triassic-k3	7	226 (45.0)	1.024 (0.012)	0.498 (0.379)	002,6	63.9/16.1	124,24	143,82	25.5/7.7	247,54	1	239/36ov	a
QB69	red lutites	Late Triassic-k3	11	149 (41.9)	1.048 (0.017)	0.701 (0.280)	135,11	53.5/23.7	317,14	239,50	28.2/23.8	088,68	1	069/60	a
Bicorb Half-graben															
QB06	lutites	Low-midd Mioce	11	79.1 (19.8)	1.014 (0.006)	0.053 (0.338)	009,77	40.9/27.0	338,24	208,12	46.4/28.3	232,32	3	330/55	a
QB08	grey lutites	Upper Miocene	12	37.5 (19.7)	1.015 (0.010)	0.102 (0.395)	322,31	23.6/12.7	144,0	085,42	47.2/12.5	054,45	3	335/30	a
QB09	lutites/fine sandst	Low-midd Mioce	11	41.8 (23.1)	1.027 (0.019)	0.284 (0.458)	281,66	19.9/6.6	315,5	094,24	49.0/13.2	048,34	3	334/70	a
QB50	oran. mudst/sandst	Low-midd Mioce	11	126 (17.9)	1.008 (0.005)	0.088 (0.502)	033,11	30.8/22.6	214,14	125,13	31.9/15.3	032,15	3	336/44	a
QB57	oran.mudst/sandst	Low-midd Mioce	10	115 (23.2)	1.009 (0.005)	0.179 (0.411)	067,51	68.2/17.5	336,17	302,25	27.3/10.5	120,69	1	123/86ov	a
QB58	grey mudst/sands	Upper Miocene	11	122 (12.8)	1.011 (0.003)	0.706 (0.237)	038,1	50.3/6.8	218,2	293,84	9.2/3.5	319,78	1	340/07	a
QB59	mudstones/limest	Upper Miocene	12	53.0 (18.8)	1.007 (0.003)	0.000 (0.407)	295,0	27.5/15.0	115,3	026,82	19.3/9.8	009,80	3	318/03	a
Quesa Half-graben															
QB04	orange lutites	Low-midd Mioce	12	72.9 (33.1)	1.025 (0.010)	0.613 (0.249)	143,36	54.9/13.6	324,8	293,49	31.6/12.9	216,65	1	149/45	a
QB14	oran.mudst/sandst	Low-midd Mioce	10	111 (75.3)	1.021 (0.009)	0.563 (0.356)	241,13	48.3/8.6	240,5	014,72	8.7/6.4	356,78	1	221/13	a
QB17	lutites	Low-midd Mioce	10	56.0 (15.0)	1.039 (0.014)	0.535 (0.335)	200,8	31.6/7.7	199,0	068,78	17.8/7.9	109,75	2	163/10	a
QB19	or-yell.muds/sand	Low-midd Mioce	12	75.9 (27.2)	1.030 (0.008)	0.413 (0.213)	113,11	9.8/5.2	293,6	326,77	5.7/4.4	057,80	2	108/17	a
QB53	grey mudstones	Upper	14	17.7	1.024	0.108	133,44	53.3/15.0	133,38	036,7	33.6/18.2	037,7	4	124/06	a

		Miocene		(7.22)	(0.011)	(0.404)									
Other Miocene outcrops															a
QB11	fine sandstones	Low-midd Mioce	10	1140 (201)	1.029 (0.006)	-0.281 (0.228)	057,13	3.7/3.1	056,5	159,43	21.6/3.3	153,51	3	015/10	a
QB16	oran.lutites/sandst	Low-midd Mioce	12	69.7 (22.5)	1.017 (0.006)	0.376 (0.256)	341,46	42.6/9.3	016,19	216,28	15.9/8.9	160,67	1	063/56	a
QB61	oran.mudst/sandst	Low-midd Mioce	10	73.2 (35.6)	1.012 (0.004)	0.253 (0.345)	036,64	44.2/17.1	022,18	178,21	24.4/13.5	161,67	1	010/48	a
QB71	oran.mudst/sandst	Low-midd Mioce	11	101 (16.1)	1.015 (0.003)	0.140 (0.292)	343,7	19.5/10.6	343,1	143,83	12.7/8.7	249,81	2	281/13	a

n = number of measured AMS specimens (one measured specimen per core)

$K_m = (K_{max} + K_{int} + K_{min}) / 3$ (mean susceptibility, in 10^{-6} SI units)

$P_j = \exp \{2[(\eta_1 - \eta)^2 + (\eta_2 - \eta)^2 + (\eta_3 - \eta)^2]\}^{1/2}$ (Jelinek, 1981)

$T= [2(\eta_2 - \eta_3) / (\eta_1 - \eta_3)] - 1$ (shape factor; Jelinek, 1981)

D, I (kmax)=Declination and inclination of K_{max}

For each site the line shows the arithmetic means of the individual site mean values

(standard deviation in parenthes)

K_{max} and K_{min}, mean (trend/plunge) of the magnetic lineation and of the pole of the magnetic foliation (Jelinek, 1977)

E11.1 (e_{12}/e_{13}), e_{12} and e_{13} are half confidence angles of K_{max} from Jelinek's statistics

E11.3 (e_{13}/e_{23}), e_{13} and e_{23} are half confidence angles of K_{min} from Jelinek's statistics

a=Simple restoration of bedding to the horizontal

b=1. Fold axis to horizontal correction + 2. Restoration of resulting data to the horizontal

c=1. Local dip correction + 2. Restoration of resulting data to the horizontal

Table 2

Site	Lithology	Age	n	LT-Km	LT-P'	LT-T
QB03	red lutites	Late Triassic	8	459 (153)	1.038 (0.022)	0.675 (0.170)
QB18	red lutites	Late Triassic	8	594 (70.7)	1.045 (0.031)	0.620 (0.218)
QB04	brown lutites	Early Miocene	8	143 (64.9)	1.018 (0.01)	0.646 (0.327)
QB08	pale grey lutites	Late Miocene	7	152 (48.7)	1.013 (0.003)	0.639 (0.145)
QB19	brown lutites	Early Miocene	8	204 (61.3)	1.024 (0.007)	0.539 (0.145)

n = number of measured LT-AMS specimens

For each site the line shows the arithmetic means of the individual site mean values

(standard deviation in parenthes)

For K_m, Pj and T, see description on Table 1.

Highlights

-Magnetic fabrics to assess the applicability of AMS in the study of salt structures.

-AMS, low-temp AMS, AARM and rock-mag experiments to analyse the main AMS carriers.

-Rocks from the studied salt-walls show magnetic ellipsoids linked to deformation.

-Magnetic lineations from the studied salt structures are not related to salt flow.